CONFOCAL IMAGE-BASED COMPUTATIONAL MODELING OF NITRIC OXIDE TRANSPORT IN A RAT MESENTERIC LYMPHATIC VESSEL

A Thesis

by

JOHN TYLER WILSON

Submitted to the Office of Graduate Studies of
Texas A&M University
in partial fulfillment of the requirements for the degree of

MASTER OF SCIENCE

Approved by:

Chair of Committee,	James E. Moore, Jr.
Committee Members,	Michael R. Moreno
	David C. Zawieja
Head of Department,	Gerard L. Cote

December 2012

Major Subject: Biomedical Engineering

ABSTRACT

The lymphatic system plays an important role in protein and solute transport as well as the immune system. Its functionality is vital to proper homeostasis and fluid balance. Lymphatic fluid (lymph) may be propelled by intrinsic (active) vessel pumping or passively. With regard to the former, nitric oxide (NO) is known to play an important role in lymphatic vessel contraction and vasodilation. Lymphatic endothelial cells (LECs) are sensitive to shear and increases in flow have been shown to cause enhanced production of NO by LECs. Additionally, high concentrations of NO have been experimentally observed in the sinus region of mesenteric lymphatic vessels. The goal of this work was to develop a computational flow and mass transfer model using physiologic geometries obtained from confocal images of a rat mesenteric lymphatic vessel to determine the characteristics of NO transport in the lymphatic flow regime.

Both steady and unsteady analyses were performed. Steady models were simulated by prescribing fully developed velocity profiles ranging from 0.5 mm s^{-1} to 7 mm s^{-1} as the inlet boundary conditions. Unsteady simulations were generated using a velocity profile taken from experimental data from *in situ* experiments with rats. Production of NO was shear-dependent; basal cases using constant production were also generated.

Simulations revealed areas of flow stagnation adjacent to the valve leaflets, suggesting the high concentrations observed here experimentally are due to lack of convection in this region. LEC sensitivity was found to alter the concentration of NO in

the vessel, and the convective forces were found to profoundly affect the concentration of NO at a Peclet value greater than or equal to approximately 61. The quasi-steady analysis was able to resolve wall shear stress within 0.15% of the unsteady case. However, the percent error between unsteady and quasi-steady conditions was higher for NO concentration (approximately 6.7%).

ACKNOWLEDGEMENTS

I would like to thank my committee chair, Dr. James Moore, and my committee members, Dr. Michael Moreno and Dr. David Zawieja for their guidance and support throughout the course of this research.

I am grateful to all of my friends and colleagues at Texas A&M University who have supported me throughout my time here. In no particular order: Dr. Ellie Rahbar, Dr. Will Richardson, Mohammad Jafarnejad, Samira Jamalian, Meagan Saldua, Jennifer Rodriguez, Andrea Muschenborn, Merene Philip, Dr. Danika Hayman, and Gus Hellerstedt.

Finally, I would never have gotten where I am today without the love and support of my family. In particular, I would like to thank my mother, Lisa Flores, and my grandmother, Bobbie Myers, for always believing in me even when I sometimes doubted myself.

NOMENCLATURE

*	dimensionless quantity
α	thermal diffusivity
γ	parameter that characterizes LEC sensitivity to WSS
CFD	computational fluid dynamics
D_{ij}	diffusion coefficient of NO in aqueous solution
k_{NO}	pseudo-second order auto-oxidative NO reaction rate
LEC	lymphatic endothelial cell
NO	nitric oxide
Pe	Peclet number
r	radial position
R	representative radius of the lymphatic vessel
Re	Reynolds number
RMS	root-mean-square
R_{NO}	NO production rate
$R_{NO,Max}$	maximum nitric oxide production rate
t	time
$\vec{v}$	3D velocity field
V_o	average inlet velocity
W_o	parameter that dictates saturation level of production by LECs
WSS	wall shear stress

WSS_{axial}	axial wall shear stress

TABLE OF CONTENTS

Page

LIST OF FIGURES

Page

LIST OF TABLES

Page

1. INTRODUCTION

The lymphatic system is an expansive vascular network that plays a vital role in fluid homeostasis and physiologic function within the body. It is responsible for the transport of fluid from the interstitial spaces to the venous return. Its dysfunction could result in a number of pathologies including lymphedema, or swelling of fluid within the interstitial spaces. Additionally, it is important for proper immune system functionality and protein balance.

Terminal lymphatics composed primarily of endothelial cells passively take up fluid and solutes from the interstitial spaces. Eventually, this initial network of vessels gives rise to the collecting lymphatics which are generally tubular vessels segmented by bi-leaflet valves encapsulated by a bulbous sinus region. Lymph (largely aqueous with low concentrations of proteins and cells) is propelled through the collecting lymphatics via two primary modes: intrinsic and extrinsic mechanisms. The former, also known as active transport, is the result of lymphatic muscle cell contraction, while the latter involves external mechanisms such as movement of skeletal muscle or other surrounding tissues.

Nitric oxide (NO), a known vasodilator, has been shown to influence lymphatic pumping. Enhanced wall shear stress (WSS) results in greater amounts of endothelial nitric oxide synthase (eNOS) and hence NO in human lymphatic endothelial cells (LECs) [1]. Bohlen *et al*. found an approximately two fold higher concentration of NO encapsulated by the bulbous surface of the valve region of the lymphatics compared to

that of the tubular portion [2]. Despite experimental efforts to determine the transport properties of NO within the lymphatic vasculature, it is unclear why such high concentrations exist within the bulb region of lymphatic vessels. The answer to this question may lie in the nature of flow patterns in lymphatic vessels and/or the shear sensitivity of LECs.

While there are no studies that have attempted to model transport within the lymphatic system, several computational works have been conducted that model NO transport within a parallel plate flow chamber or a simplified model of the microcirculation [3-5]. Other models developed for the lymphatic system are simply lumped-parameter [6], one-dimensional [7], or do not properly take into account the geometry of the valve region [8].

The main aim of this study was to characterize the distribution of NO within a physiologic model of a lymphatic vessel obtained from confocal images in response to various convective flow regimes and degrees of LEC sensitivity to shear. In particular, we wanted to identify the importance of convective transport of NO within the lymphatic vasculature and determine if the high concentrations in the sinus region observed in an experimental setting may be attributed to flow-mediated factors, higher LEC numbers, or some combination. While there have been experimental studies that have quantified NO concentration within the lymphatics [2], to the authors' knowledge this is the first study that has attempted to computationally model the transport of NO within a 3-D model of a lymphatic vessel.

2. METHODS

2.1 Vessel Geometry

Pentobarbital (50 mg mL^{-1}, 50 mg kg^{-1}, IM) was used to anesthetize male Sprague-Dawley rats (280-380 g) and an abdominal incision was made to expose the mesenteric lymphatic bed. Appropriate sections of the mesentery were isolated and all living cells were fluorescently tagged by intraluminally loading the vessel with CellTracker Green CMFDA (25 μM, MolecularProbes). After cannulation, the vessel was placed in a CH2 Microvessel Chamber (Living Systems Instrumentation) in Ca^{2+}-free physiologic saline solution to prevent contractions. The inlet and outlet of the isolated vessel were attached to pipettes leading to separate reservoirs of PBS where an axial pressure difference of -5 cmH_2O (P_{out}-P_{in}) at an average pressure of 3.5 cmH_2O was enforced to ensure an open valve configuration. Image slices approximately 2.5 μm apart for the full depth of the vessel were obtained via confocal microscopy (Nikon, Eclipse TE2000-E).

The stacks of confocal images were imported into Scan IP/FE (Simpleware, Exeter, UK) and were smoothed, filtered, and reconstructed into a 3-D surface mesh of the vessel fluid region (Figure 1). In particular, recursive Gaussian and salt-and-pepper filters were used to smooth the images and reduce noise. The surface mesh was then saved in *.stl format for later computational fluid dynamics (CFD) analysis.

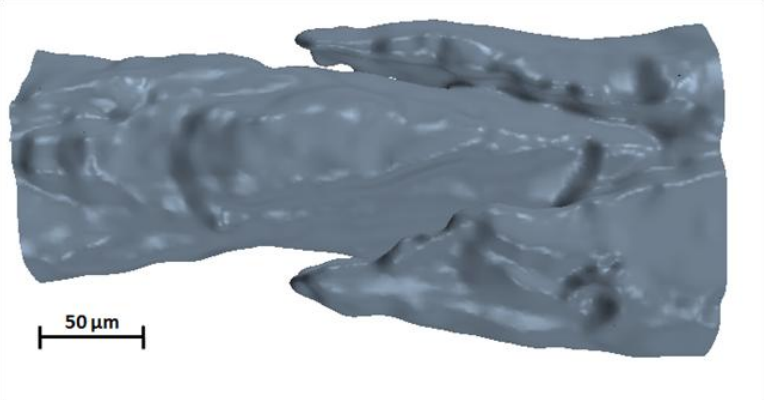

Figure 1. Geometry of the fluid region of the rat mesenteric lymphatic vessel. 200 µm extensions (extensions not shown in illustration) were added at both the inlet and outlet of the vessel to accommodate flow simulations.

Employing the analogy between mass and energy transfer, the dimensionless temperature values were used to model the concentration of NO in the vessel. The computational grid was divided into control volumes and the Navier-Stokes and Conservation of Energy equations were solved for each cell. To ensure accuracy in our analysis, the Lewis relation [9] was employed and α/D_{ij} was specified as unity, where α is thermal diffusivity and D_{ij} is the diffusion coefficient of NO in aqueous solution. Thus, the energy solutions have the same shape as that of the mass transfer. Table 1 shows the values for the concentration and thermal parameters.

Table 1. Description of constant parameters used in the simulations with corresponding thermal equivalents. α/D_{ij} was specified as unity in order to ensure accuracy in the analogous assumption between mass and energy transfer.

Concentration Parameters		
Symbol	*Value, Units*	*Description*
D_{ij}	3.3×10^{-5} cm^2 s^{-1}	diffusion coefficient of NO in water
k_{NO}	7.56×10^{-6} nM^{-1}s^{-1}	pseudo-second order auto-oxidative NO reaction rate
$R_{NO,Max}$	0.0033 µM cm s^{-1}	max NO production rate
ρ	1000 kg m^{-3}	density of lymph
R	50 µm	representative radius
Equivalent Thermal Parameters		
K	0.0138 W m^{-1}·K^{-1}	thermal conductivity
c_p	4181.72 J kg^{-1}·K^{-1}	specific heat
k_T	1.38 W m^{-3} K^{-1}	pseudo-second order energy consumption rate

All mass transfer values were matched from the literature [4] and correspond to NO in aqueous solution. Thus, all computational details described hereafter will only involve concentration values.

2.2 Flow and Concentration Equations

Both steady and time-dependent simulations were performed using the commercially available software Star-CCM+ (CD-adapco; Melville, NY). The software employs the finite volume approach that uses 2nd order discretization to solve for flow and energy on the computational grid. The thermal results were non-dimensionalized to obtain the analogous concentration solution.

Lymph was assumed to be a Newtonian and incompressible fluid with a dynamic viscosity, µ, of 0.9 cP and density, ρ, of 1 g cm^{-3}. Transport of NO is governed by the Advection-Diffusion-Reaction equation:

$$\frac{\partial C_{NO}}{\partial t} = -\vec{v} \bullet \vec{\nabla} C_{NO} + D_{ij} \vec{\nabla}^2 C_{NO} - k_{NO} C_{NO}^2 , \quad (1)$$

where $\vec{v}$ is the velocity field, C_{NO} is the concentration of NO, t is time, and k_{NO} is the pseudo-second order auto-oxidative NO reaction rate. A sigmoidal relationship between NO production and axial WSS was used as the flux boundary condition for NO production at the wall of the vessel (Eqn. 2):

$$R_{NO}(r) = \frac{R_{NO,Max}}{1 + \gamma \exp(-W_o \left| WSS_{axial} \right|)} \quad (2)$$

where R_{NO} is the production rate of NO, $R_{NO,Max}$ is the maximum production rate of NO corresponding to the rate used by Plata *et al*. [4] when modeling arterial endothelial cell production, WSS_{axial} is axial WSS, r is the radius, and γ and W_o characterize LEC sensitivity to shear. This function represents an increase in production in response to WSS, but at a certain value of axial WSS (termed the "saturation point") the LECs can no longer produce at a higher rate with further elevation in shear (Figure 2). Furthermore, an increase or decrease in the parameter W_o results in this saturation point occurring at a higher or lower value of axial WSS.

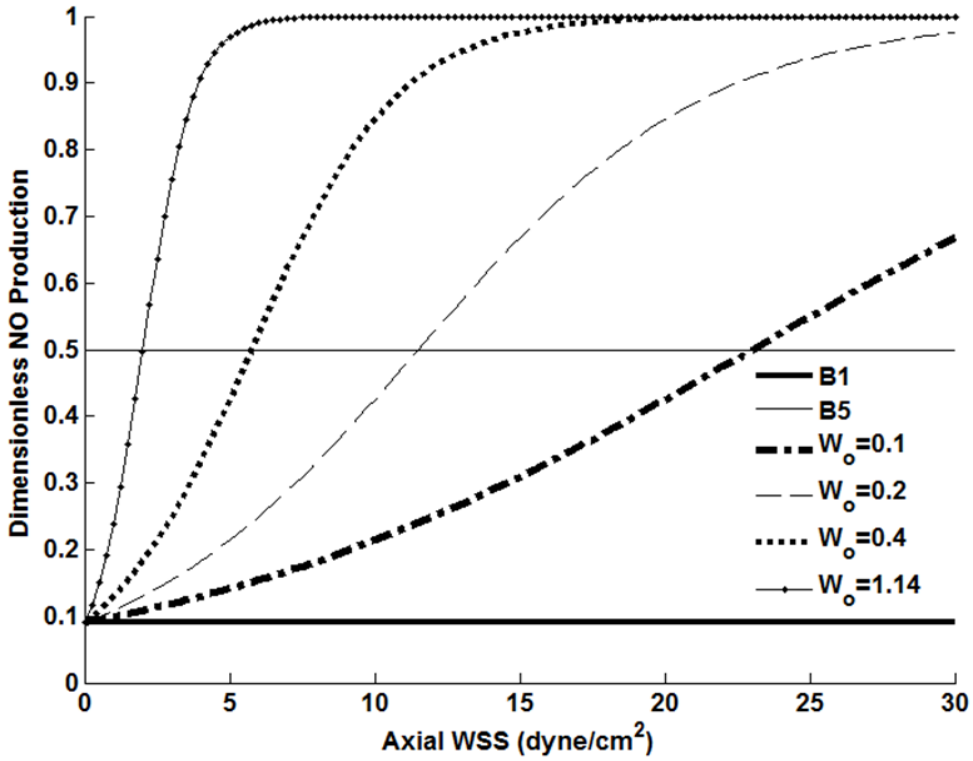

Figure 2. Range of NO production values fixed with γ=10. For shear dependent cases, W_o was varied from 0.1 to 1.14 corresponding to increasing levels of LEC shear sensitivity. Basal level productions B1 and B5 correspond to dimensionless production values of 0.09 and 0.5, respectively.

In this study, W_o was varied to determine the effect of different saturation points on the concentration of NO within the lumen of the vessel. It should be noted that the maximum production was assumed to be 11 times that of the basal level (e.g. γ=10). The parameter γ was not varied because its effect on overall production rate is not as impactful as that of W_o [4]. Simulations were also run using constant NO production boundary conditions with dimensionless values of 0.09 and 0.5 corresponding to the parameters B1 and B5, respectively.

Variables were converted to dimensionless form in the following manner:

$$v^* = \frac{\vec{v}}{V_o}, \tag{3}$$

$$r^* = \frac{r}{2R}, \tag{4}$$

$$C^* = \frac{C_{NO} D_{ij}}{R_{NO,Max}\, 2R}, \tag{5}$$

$$k_{NO}^* = \frac{k_{NO} (2R)^2 R_{NO,Max}}{D_{ij}^2}, \tag{6}$$

$$t^* = \frac{t}{t_o}, \tag{7}$$

$$R_{NO}^* = \frac{R_{NO}}{R_{NO,Max}}, \tag{8}$$

where V_o is the average value of the parabolic inlet velocity, R is the representative radius at the inlet of the lymphatic vessel, and t_o is the characteristic time equivalent to 9 s. Inserting Equations (3-8) into Equation (1) results in the following governing dimensionless equation:

$$\frac{\partial C^*}{\partial t^*} = -Pe\vec{v}^* \bullet \vec{\nabla} C^* + \vec{\nabla}^2 C^* - k_{NO}^* C^{*2}, \tag{9}$$

where Pe is the Peclet number equilavant to $2RV_o/D_{ij}$.

2.3 Model Geometry and Computational Inputs

200 μm long inlet and outlet extensions were added to the geometry to facilitate the application of boundary conditions. The extrusion lengths were varied to determine the effect on velocity and concentration within the lumen of the vessel and it was found

that the lengths aforementioned were optimal. In particular, the selected inlet length allowed for the development of a 3-D parabolic velocity profile.

Table 2. Range of velocities and dimensionless numbers used for steady simulations. Note that Re is less than one for all cases, suggesting the important role of viscous forces in the lymphatic flow regime.

V_o ($mm\ s^{-1}$)	*Pe*	*Re*
0.5	15	0.06
1.0	30	0.11
2.0	61	0.22
3.0	91	0.33
4.0	121	0.44
5.0	152	0.56
6.0	182	0.67
7.0	212	0.78

A parabolic velocity profile was implemented at the inlet with average velocities ranging from 0.5-7.0 mm s^{-1} that are in the physiologic range of velocities observed during *in situ* experiments [10] (Table 2). Note the Reynolds number, Re, is defined as $\rho V_o 2R/\mu$. To determine the validity of a quasi-steady anlysis, an unsteady case was simulated using an experimentally obtained velocity profile [10] (Figure 3). Instantaneous WSS and NO values taken at different time points were compared to steady simulation results performed at the same average inlet velocity values.

A static concentration of C^*_{NO} =0.3 corresponding to a dimensional concentration of 100 nM was applied as a Dirichlet boundary condition at the inlet of the vessel. The outlet concentration was extrapolated from adjacent core cells using a reconstruction gradient. However, when inflow or recirculation due to negative velocity values occurred, the characteristic concentration of C^*_{NO} =0.3 was implemented at the outlet (now effectively the inlet). The extruded walls of the entrance and exit regions of the vessel were set to a zero flux in order to prevent interaction with concentration profiles within the physiologically relevant portion of the geometry. In order to minimize transients for the unsteady case, the simulation was initialized at the steady-state solution for the velocity at the first time-step in the numerical scheme. Additionally, residuals for iterations in the steady case and inner iterations for the unsteady case were allowed to reach a value on the order of 10^{-4} to ensure convergence.

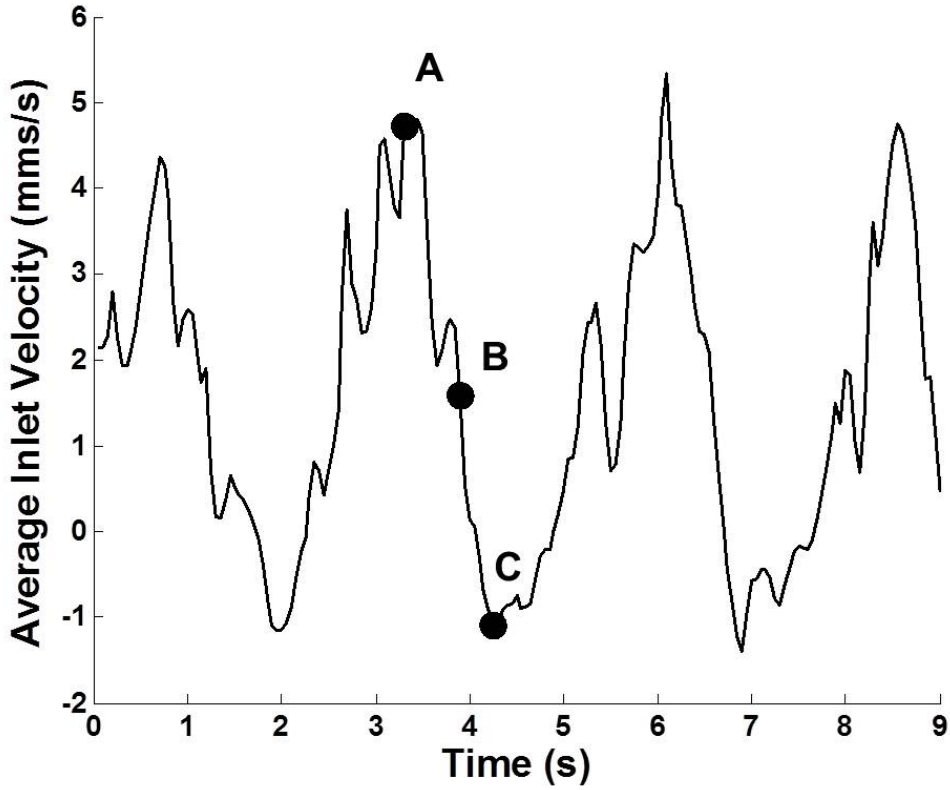

Figure 3. Transient velocity from a rat mesenteric lymphatic vessel used for time-dependent simulations. The raw waveform taken from the literature [10] was interpolated using a 0.05 s time step resulting in a velocity profile consisting of values obtained through a sampling frequency of 180 points for 9.0 s. A, B, and C are locations along the velocity where instantaneous WSS and NO values were extracted. These points correspond to the maximal, transitional, and peak values of velocity, respectively.

2.4 Mesh Independence

Mesh independence was investigated by comparing steady flow axial WSS values (fully developed inlet condition) in meshes with 95,149, 201,056, 385,080, and 1,202,744 volumetric cells. Less than 6% RMS error in axial WSS was found between the 385,080 and 1,202,744 cell meshes (Figure 4), which compares well with the criteria set forth by Ethier *et al.* in modeling flow in coronary arteries [11].

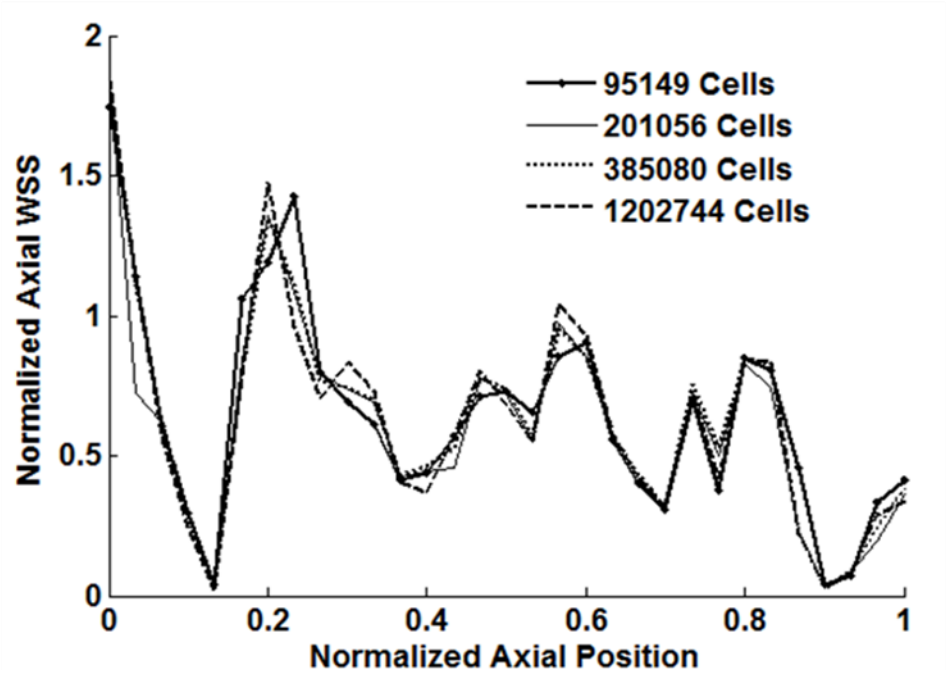

Figure 4. Mesh indpendence study using WSS as convergence criteria in the rat mesenteric lymphatic vessel. The steady WSS values were normalized by the inlet Poiseuille flow value of WSS and plotted along the wall of the vessel. A parabolic inlet velocity was used in each case.

Therefore, the 385,080 cell mesh was used for all results. For the time-dependent case, the raw velocity was filtered and simulations were performed using 72, 180, and 900 time points corresponding to 0.125 s. 0.05 s, and 0.01 s timesteps, respectively (Figure 5).

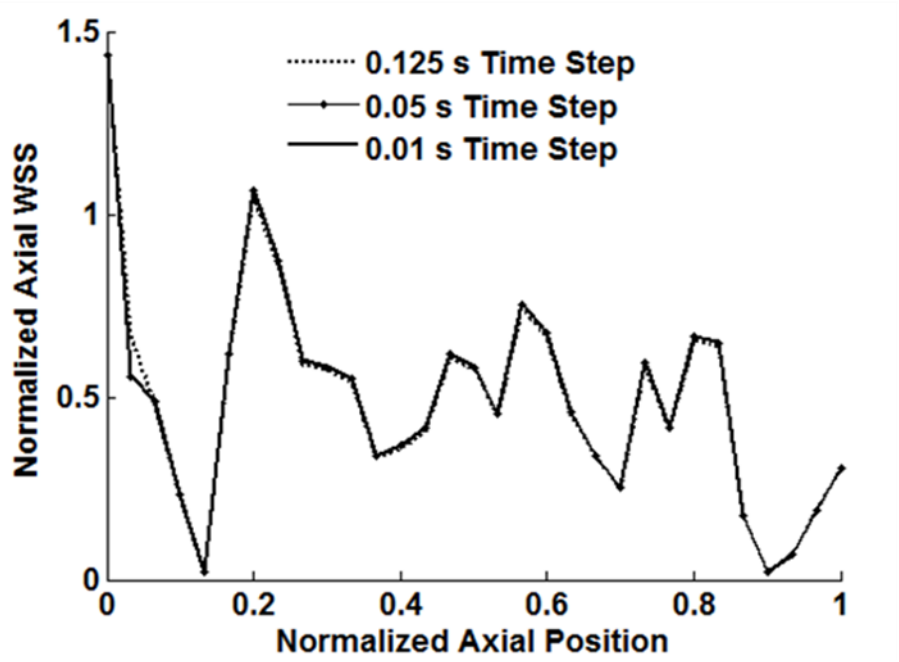

Figure 5. Temporal resolution study using WSS as convergence criteria in the rat mesenteric lymphatic vessel. The time-averaged WSS values were normalized by the inlet time-averaged Poiseuille flow value of WSS and plotted along the wall of the vessel.

Increasing the number of time steps beyond 180 resulted in less than 0.14% difference in time-averaged WSS values. Therefore, a time step of 0.05 s was used to generate the results presented herein.

3. RESULTS

3.1 Steady Simulation Results

Velocity streamlines revealed areas of flow stagnation adjacent to the valve leaflets in the sinus region (Figure 6). While these appear to be vortex-like in shape, it should be noted that the absolute value of velocities in this region were less than 0.03 mm/s compared to an average inlet velocity of 2.0 mm/s.

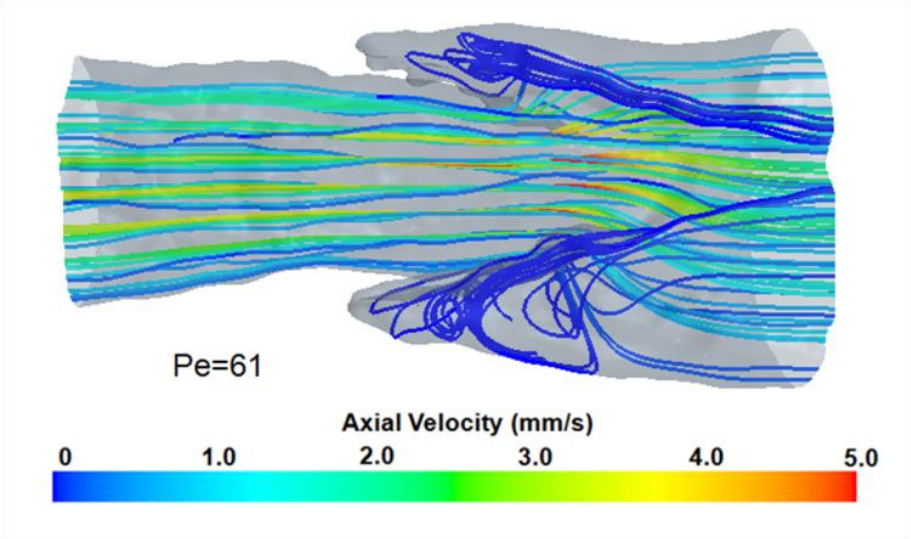

Figure 6. Respresentative streamlines for a simulation run at Re=0.22. Areas of flow stagnation were observed adjacent to the valve leaflets. Although these appear vortex-like in nature, these are regions of essentially zero velocity.

The maximum shear stress occurred near the trailing ends of the lymphatic valve leaflets and was 12.0 dyne cm^{-2} for an imposed Pe value of 91 (Figure 7 Top). Contours of NO production (Figure 7 Middle and Bottom) revealed higher production in areas of

elevated WSS dictated by the sigmoidal function used for the flux boundary condition of NO. When W_o was set to a lower value (Figure 7 Middle), the LECs were less sensitive to shear compared to simulations run at a higher value of W_o (Figure 7 Bottom). Higher values of W_o caused larger surface areas of the vessel wall to reach the maximum value of production compared to simulations run at the lower value of W_o.

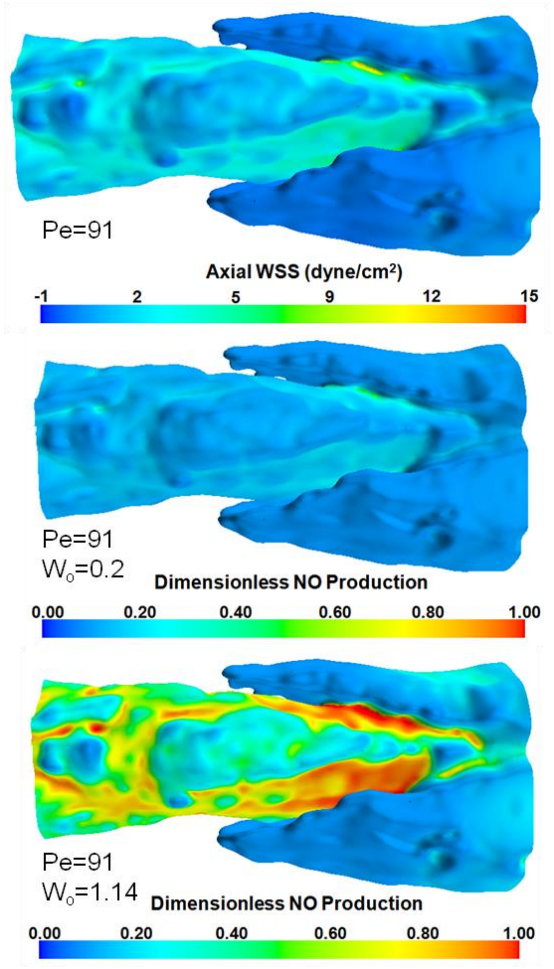

Figure 7. WSS and corresponding NO production distributions. Top: Distribution of axial WSS for Pe=91; Middle: Dimensionless NO Production for Pe=91 and Wo=0.2; Bottom: Dimensionless NO Production for Pe=91 and Wo=1.14.

Despite higher production levels in the simulations run with large Pe values, the prodominant role of convective forces was evident from the diminished concentration within the lumen of the vessel. The highest concentrations were found near the valve leaflet insertions in areas of flow stagnation and low WSS (Figure 7 Top, Middle, and Bottom). Simulations run at lower Pe numbers (Figure 8 Top) resulted in higher concentrations than those run at elevated Pe values (Figure 8 Bottom).This may be attributed to NO being washed out of the lumen of the vessel due to higher convective forces in the latter case.

The flow-mediated decrease in concentration was also evident in the areas of flow stagnation near the valve leaflets. After Pe $\geq$ 61, the concentration at the wall did not change substantially as is evident by comparing the two simulations run at the higher Pe values (Figure 8 Middle and Bottom Panels). The concentrations near the center of the vessel were generally low due to dominant convective forces (Figure 9). Closer to the wall, higher concentrations were observed with higher Pe values (Pe > 61) due to increased shear-sensitive production. However, diffusive forces dominated in the simulations run at Pe values less than 30 and high values in concentration were present across all radial values, particularly evident in the case Pe=15.

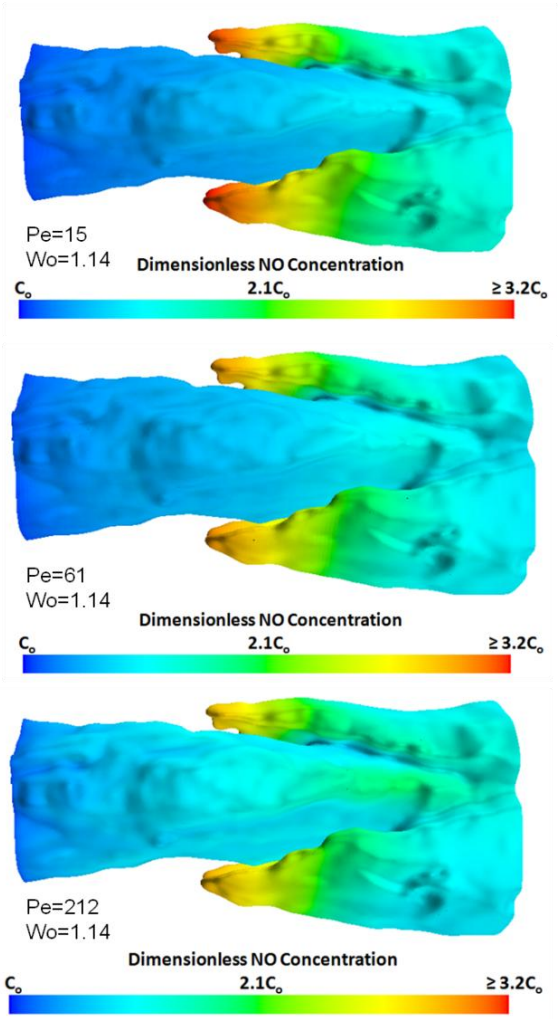

Figure 8. Contours of NO at the wall of the vessel for various Pe values. Top: Surface concentration for Pe=15 and Wo=1.14; Middle: Surface concentration for Pe=61 and Wo=1.14; Bottom: Surface concentration for Pe=212 and Wo=1.14. Increasing the average Pe value resulted in less wall concentration, however enhanced Pe values beyond Pe=61 up until Pe =212 only resulted in an RMS percent difference in NO concentration of 3.7%.

Generally at low Pe, diffusion played more of a role in transport and there was a build-up of NO, similar to the observed effect in the sinus region where flow stagnation occurred.

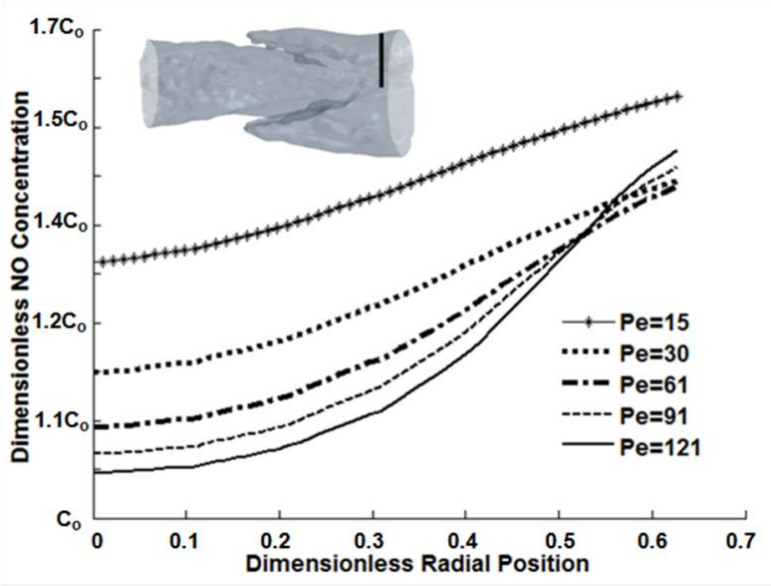

Figure 9. Concentration plotted in the radial direction at an axial location downstream of the valve leaflets.

The inclusion or lack of shear-dependent NO production had profound effects on concentration profiles. Wall concentration decreased monotonically by as much as half over the physiologic range of Pe for the baseline B5 constant production case (Figure 10). The baseline B1 case showed smaller, but still monotonic, decreases in wall concentrations with increasing Pe. This finding was consistent at all wall locations in the model. However, the simulations where production was shear-dependent resulted paradoxically in the wall concentration being less sensitive to Pe, and thus shear. The concentration profiles that result from shear-sensitive NO production began to decrease initially and then increased with increasing Pe. This initial decrease may be interpreted as the concentration profile being transformed from an effectively purely diffusive behavior to a predominantly convective regime. Thereafter, the slight increases in wall

concentration were due to increased production, but were offset to some degree by increased convection.

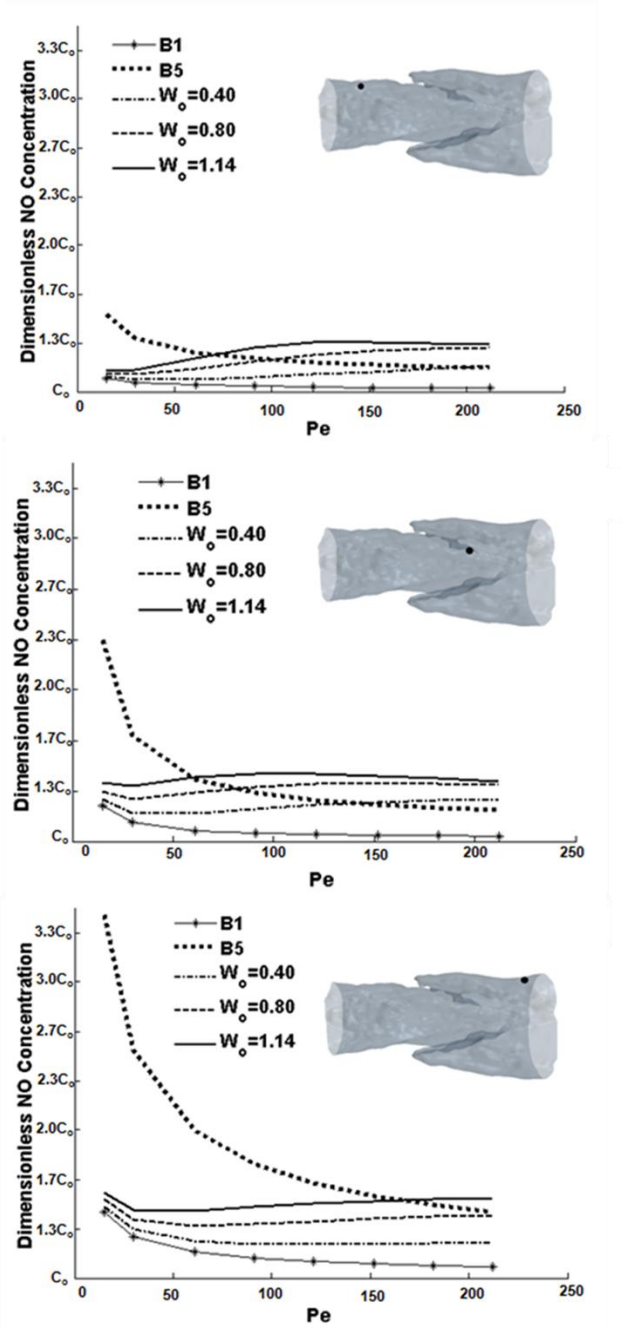

Figure 10. Concentration sampled at the wall across a range of Pe and W_o values. Top: point upstream of the valve leaflets; Middle: point of highest axial WSS; Bottom: point downstream of the valve leaflets.

3.2 Unsteady Flow

For unsteady simulations, the concentration peaked at both positive and negative peak values of WSS because the sigmoidal NO production dependence on WSS was based on the absolute value of axial WSS rather than a "directional" value (Figure 11).

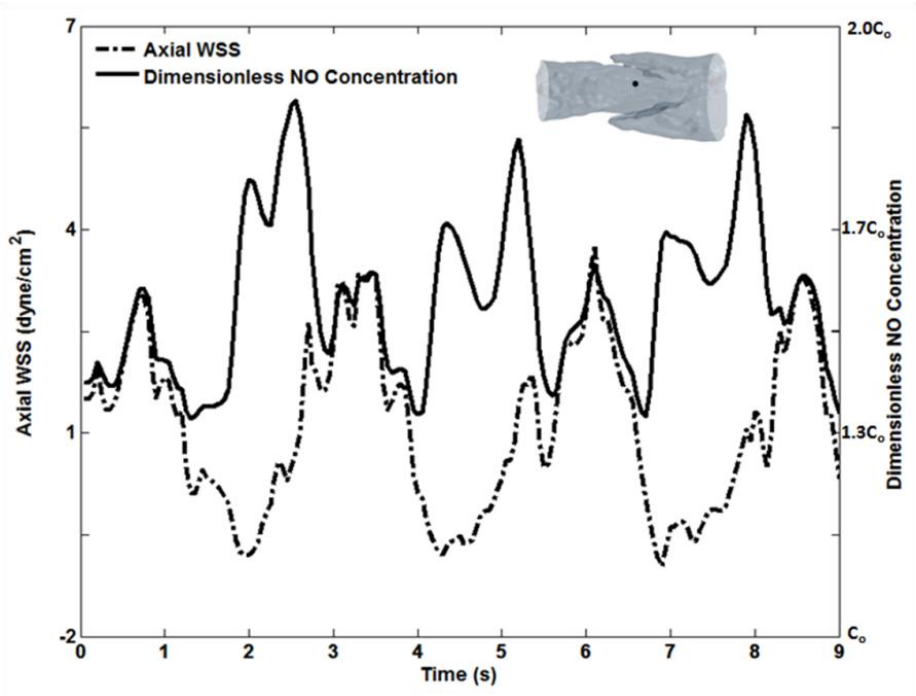

Figure 11. Concentration at the wall at a location upstream of the terminal edges of the lymphatic valve leaflets.

The peaks in concentration were higher for negative values of WSS because previously produced NO was transported from areas downstream of the valve site. Instantaneous concentration and WSS results from the unsteady simulation were compared to those of quasi-steady simulations at the corresponding average inlet velocites (Figure 12).

Although many time points were compared, the results listed in Figure 12 respresent data when the flow regime was at its maximum peak (t = 3.3 s), transition into systole (t = 3.9 s) and minimum positions (t = 4.25 s).

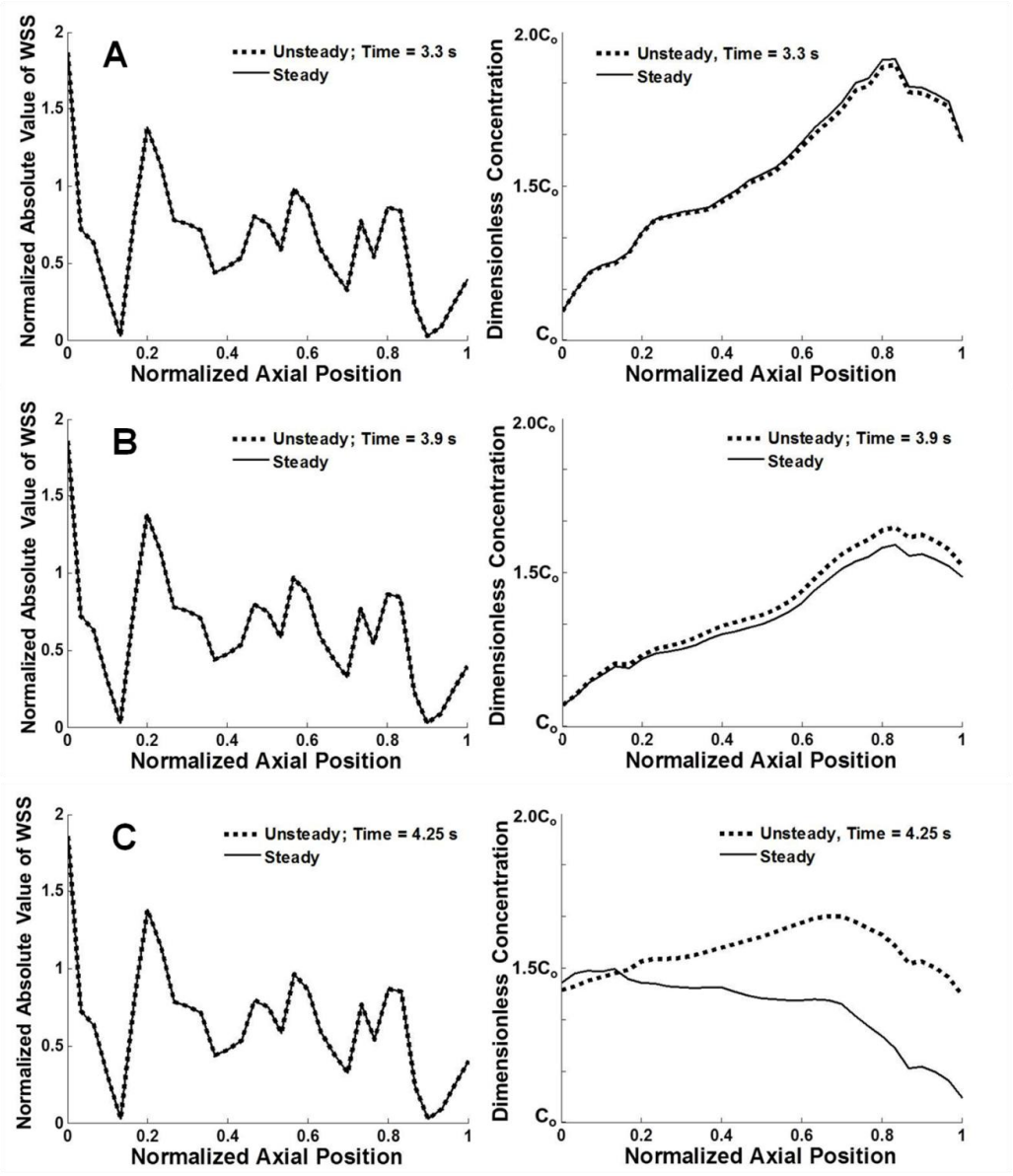

Figure 12. Comparison of steady WSS and NO values versus axial position to that of the unsteady case at time points A, B, and C correspdoning to 3.3 s, 3.9 s, and 4.25 s, respectively. WSS values were normalized to corresponding inlet Poiseuille value of WSS.

WSS values across all time points were resolved to less than 1% with the quasi-steady approach. However, the RMS error in concentration profiles between steady and unsteady cases increased with decreasing velocity (Table 3). For example, differences between steady and unsteady concentrations were 0.40% for the simulation run at peak velocity (t = 3.3 s) compared to 6.70% for the simulation run at the minimum velocity (t = 4.25 s).

Table 3. RMS Error in steady versus unsteady simulations.

Time (s)	*Velocity (mm/s)*	*% RMS WSS Error*	*%RMS Concentration Error*
3.3	4.70	0.60	0.40
3.9	1.58	0.13	1.14
4.25	-1.08	0.04	6.70

Instantaneous concentration values taken at a time when the velocity was small or at a minimum had lingering NO within the lumen of the vessel that had not been transferred away due to the increasingly diffusive nature of the transport scheme. This lingering NO in the unsteady cases was not found in the quasi-steady simulations and thus contributed to the percent difference between the two. Based on these findings, unsteady concentration results generally agreed better with steady results in flow regimes with an overall higher velocity.

4. DISCUSSION

The study presented herein investigated the effects of fluid dynamics and LEC sensitivity on the concentration of NO within the lumen of a lymphatic vessel. This is the first time such a study was conducted on a model obtained from confocal images of a live lymphatic vessel. By implementing shear-sensitive boundary conditions for the production of NO, we were able to understand how the sensitivity of LECs may play a role in the concentration of NO. Additionally, we showed that areas of high concentration exist within the sinus regions near the valve leaflets as observed by Bohlen *et al*. [2]. Our results further validated that a quasi-steady analysis is appropriate, particularly for cases where the velocities are elevated.

While the average values of shear within the lymphatic flow regime are approximtely 0.64 dyne cm^{-2} [10], the peak values of shear quantified in simulations were generally comparable to WSS values calculated for large arteries [12]. Additionally, high concentrations have been observed experimentally near the valve leaflets in the sinus area, but it was unclear as to whether this phenomena was due to high surface area with more LECs to produce NO, higher production rates in general at this site, or whether it is flow mediated. Furtheremore, experiments have shown that an increase in shear results in increased production of NO by LECs [1]. We found that LECs in areas of flow stagnation observed in representative velocity streamlines produced at a much lower rate than do LECs in the higher shear areas of the vessel. Despite the low production rates in this area, there was substantially more NO present in

this region compared to areas of high production, suggesting the high concentration in this area observed experimentally is flow-mediated and due to stagnation as opposed to a higher value of NO production. Additionally, the extremely low levels of production and highly diffusive forces seem outweigh the concept that high surface area of LECs is the sole cause of the enhanced NO levels.

Furthermore, convection plays a major role in NO transport not only at the wall, but also within the lumen of the vessel. The local Pe numbers generated toward the center of the vessel were much greater than those at the wall and resulted in diminished NO in this region. High concentrations at low Pe values were observed for cases where the basal level production was set to the B5 constant production, which intuitively does not make sense because experiments have shown that higher concentrations of NO increase with elevation in shear [2]. Thus, this model further supports shear-dependent production of NO by showing that situations where production is constant are physiologically not germane. Additionally, there were no substantial increases in concentration after $Pe \geq 61$, suggesting that the role of convection begins to take more of an effect in the transport scheme at this point. Note that Pe=61 should not be interpreted as any "critical value" at which convection overcomes diffusion, but simply an approximate location at which the role of convection becomes more apparent.

We have futher shown that the percent difference in WSS between instantaneous values taken from unsteady and quasi-steady simulations differ by less than 1% over a range of velocity values, suggesting that a quasi-steady approach is more than adequate for resolving the fluid dynamics for this geometry. An analysis comparing concentration

profiles between quasi-steady and unsteady velocity simulations revealed increasing percent error with decreasing velocity. This was attributed to lack of transport of NO for the unsteady case out of the computational domain of interest in lower Pe simulations. However, when Pe reached a certain value, these diffusive forces were no longer significant and the quasi-steady and unsteady concentrations were quite similar, resulting in a decrease in percent error between the two. Since the range of velocities investigated under quasi-steady conditions in this study were all in the positive range (no backflow or negative velocities), the conclusions from these findings should correlate well to results if a transient velocity profile with corresponding positive velocities were implemented.

A few limitations should be noted when considering this model. The geometry used for all simulations was static while in reality lymphatic vessels contract and expand over time, thus the results included in this research are limited to quasi-steady and unsteady conditions in a stationary domain. The viscous nature of the fluid and laminar flow characteristics suggest this movement may be negligible and a quasi-static approach is appropriate, however future work could include dynamic movement of the valve leaflets to validate this assumption. Additionally, unsteady versus quasi-steady differences in concentration were only compared for a W_o value of 1.14, but a similar behavior is expected across all values of this parameter. Future work could also include incorporation of diffusion through the vessel wall. Consequently, it would be useful to determine whether the areas of high concentration such as as those found adjacent to the valve leaflets due to flow stagnation would have the highest amount of diffusion through

the vessel wall. This type of analysis would be dependent on the diffusivity of NO within the vessel wall.

5. CONCLUSIONS

Our results showed that high concentrations observed adjacent to the valve leaflets in experimental findings were most likely due to flow-mediated processes. Because higher values of shear led to increasing concentrations at the wall only after Pe was at or above approximately 61, simulations suggested that this value was where convective forces start to greatly affect the concentration distribution. Futhermore, this model supports the mechanism of a shear-sensitive endothelium because high levels of NO at the wall do not make physiologic sense in low velocity flow regimes as observed when comparing the basal level production cases to WSS dependent cases. Finally, a quasi-steady approach seems to be sufficent for anlaysis of WSS and NO concentration in a static model of a mesenteric lymphatic vessel.

In short, the concentrations of NO within the lymphatic vesssel were found to be sensitive to changes in the convective scheme and LEC sensitivity. Further studies could be conducted to investigate the fully dynamic system of NO transport resulting from vessel wall movement and valvular propulsion of lymph.

6. REFERENCES

[1] Kawai, Y., Yokoyama, Y., Kaidoh, M., and Ohhashi, T., 2010, "Shear stress-induced ATP-mediated endothelial constitutive nitric oxide synthase expression in human lymphatic endothelial cells," American Journal of Physiology-Cell Physiology, 298(3), pp. C647-C655.

[2] Bohlen, H. G., Wang, W., Gashev, A., Gasheva, O., and Zawieja, D., 2009, "Phasic contractions of rat mesenteric lymphatics increase basal and phasic nitric oxide generation in vivo," American Journal of Physiology-Heart and Circulatory Physiology, 297(4), pp. H1319-H1328.

[3] Fadel, A., Barbee, K., and Jaron, D., 2009, "A computational model of nitric oxide production and transport in a parallel plate flow chamber," Annals of Biomedical Engineering, 37(5), pp. 943-954.

[4] Plata, A., Sherwin, S., and Krams, R., 2010, "Endothelial nitric oxide production and transport in flow chambers: the importance of convection," Annals of Biomedical Engineering, 38(9), pp. 2805-2816.

[5] Vaughn, M. W., Kuo, L., and Liao, J. C., 1998, "Effective diffusion distance of nitric oxide in the microcirculation," American Journal of Physiology-Heart and Circulatory Physiology, 274(5), pp. H1705-H1714.

[6] Bertram, C., Macaskill, C., and Moore Jr, J., 2011, "Simulation of a chain of collapsible contracting lymphangions with progressive valve closure," Journal of Biomechanical Engineering, 133(1), p. 011008.

[7] Reddy, N. P., Krouskop, T. A., and Newell, P. H., 1977, "A computer model of the lymphatic system," Computers in Biology and Medicine, 7(3), pp. 181-197.

[8] Rahbar, E., and Moore, J. E., 2011, "A model of a radially expanding and contracting lymphangion," Journal of Biomechanics, 44(6), pp. 1001-1007.

[9] Incropera F.P., Dewitt D. P., Bergman T.L., Lavine L.S., 2007, Fundamentals of Heat and Mass Transfer, John Wiley, Hoboken, NJ.

[10] Dixon, J. B., Greiner, S. T., Gashev, A. A., Cote, G. L., Moore, J. E., and Zawieja, D. C., 2010, "Lymph flow, shear stress, and lymphocyte velocity in rat mesenteric prenodal lymphatics," Microcirculation, 13(7), pp. 597-610.

[11] Myers, J., Moore, J., Ojha, M., Johnston, K., and Ethier, C., 2001, "Factors influencing blood flow patterns in the human right coronary artery," Annals of Biomedical Engineering, 29(2), pp. 109-120.

[12] Moore, J. E., Xu, C., Glagov, S., Zarins, C. K., and Ku, D. N., 1994, "Fluid wall shear stress measurements in a model of the human abdominal aorta: oscillatory behavior and relationship to atherosclerosis," Atherosclerosis, 110(2), pp. 225-240.